Applied Physics Letters

Measurements of the magneto-optical properties of thin-film EuS at room temperature in the visible spectrum

Cite as: Appl. Phys. Lett. **120**, 251103 (2022); https://doi.org/10.1063/5.0090533
Submitted: 07 March 2022 • Accepted: 02 June 2022 • Published Online: 22 June 2022

M. L. Meretska, F. H. B. Somhorst, M. Ossiander, et al.

Applied Physics Letters ARTICLE scitation.org/journal/apl

Measurements of the magneto-optical properties of thin-film EuS at room temperature in the visible spectrum

Cite as: Appl. Phys. Lett. **120**, 251103 (2022); doi: 10.1063/5.0090533
Submitted: 7 March 2022 · Accepted: 2 June 2022 ·
Published Online: 22 June 2022

M. L. Meretska,[1,a] F. H. B. Somhorst,[1,b] M. Ossiander,[1] Y. Hou,[2] J. Moodera,[2,3] and F. Capasso[1,a]

AFFILIATIONS

[1]Harvard John A. Paulson School of Engineering and Applied Sciences, Harvard University, Cambridge, Massachusetts 02134, USA
[2]Francis Bitter Magnet Laboratory and Plasma Science and Fusion Center, Massachusetts Institute of Technology, Cambridge, Massachusetts 02139, USA
[3]Physics Department, Massachusetts Institute of Technology, Cambridge, Massachusetts 02142, USA

[a]**Authors to whom correspondence should be addressed:** mmeretska@seas.harvard.edu and capasso@seas.harvard.edu
[b]**Present address:** MESA+ Institute for Nanotechnology, University of Twente, Enschede, The Netherlands.

ABSTRACT

This paper reports on the magneto-optical properties of an electron beam evaporated EuS thin-film characterized at room temperature. The refractive index of EuS was measured using ellipsometry in the visible part of the spectrum. The dispersion curve of the Verdet constant was measured in the wavelength range between 600 and 800 nm. We fitted an analytical expression for the dispersion curve in the range of 663–785 nm. In addition, we find that the Verdet constant of thin-film EuS is one order of magnitude higher than the commonly used terbium gallium garnet crystal.

An interaction of light with matter subjected to a magnetic field leads to important physical effects, including the Faraday,[1] Kerr, Voigt,[2] and Hanle[3] effects. Often, these effects influence the polarization of the interacting light, i.e., the Faraday effect rotates light polarization upon its propagation through a material in the direction of the applied magnetic field. Many devices have been realized using these effects, including magneto-optical (MO) modulators,[4] circulators,[5] and isolators.[6] Also, this effect has been used in sensing[7] and laser technologies.[8]

It is important to note that the MO effect differs from asymmetric power transmission associated with chiral media.[9,10] The orientation of the magnetic field determines the direction of polarization rotation and breaks time-reversal symmetry. Devices based on this effect are passive, unlike approaches that rely on nonlinear effects or time modulation,[11] and are irreplaceable in certain devices.

One of the underlying reasons for polarization rotation in MO materials is the Zeeman splitting,[2] occurring when otherwise degenerated energy levels in a material are split by an applied magnetic field. While propagating in a MO material, incident light experiences a different refractive index for right circularly polarized (RCP) and left circularly polarized (LCP) light. For linearly polarized incident light, this manifests as a rotation of the light's polarization by an angle $\Delta\theta$, determined by the material's Verdet constant V, the propagation length L, and the magnetic field strength B,

$$\Delta\theta = VBL. \quad (1)$$

A challenge for current MO-based devices is that the Verdet constant of most naturally occurring materials is minuscule, requiring long propagation lengths, e.g., for achieving optical isolators. Therefore, the lateral dimension of commercially available isolators is on the order of centimeters, prohibiting their use in on-chip devices or compact optical systems. Materials with high Verdet constants will, thus, decrease the dimensions of future MO devices.

Another critical consideration for MO-based devices is absorption. Most devices operate in transmission and, thus, require low to no material absorption. This, e.g., limits the usability of metals that exhibit high Verdet constants and high absorption coefficients. Eu-chalcogenides possess remarkably high Verdet constants at visible and infrared wavelengths at low temperatures.[12] While the measurements of Eu-chalcogenides Verdet constant at room temperature have been conducted;[13] however, EuS has been overlooked. In this study, we measured the dispersion of the Verdet constant of e-beam

evaporated EuS thin films in the visible wavelength range at room temperature. In addition, we measured the real and imaginary parts of the refractive index of EuS using ellipsometry to evaluate its absorption at room temperature.

The experimental setup used for the Verdet constant measurements is shown in Fig. 1. A set of laser diodes with a central wavelength of 600 to 800 nm was used to illuminate the sample. The emission spectra of the individual diodes are shown in the supplementary material (S1). The laser diodes were mounted in a temperature-controlled diode mount (Thorlabs, LDM56), and emitted light was collimated by a lens (Thorlabs, LA1074-A-ML). A noise eater (Thorlabs, NEL02) was used to stabilize the power of the laser diodes. A neutral density filter (NDF) (Thorlabs, NE15A) after the noise eater was used to reduce the intensity of the incident light to avoid the saturation of the balanced photodetector used for signal acquisition. Before the MO material sample, the light's polarization was rotated to 45° with respect to a polarizing beam splitter (PBS) (Thorlabs, CCM1-PBS251) mounted after the sample. The MO material was placed in a magnetic field oscillating at 1 Hz with up to 0.5 T magnitude at the magnetic field probe position. A small fan was used to cool the sample and the magnet. A polarizing beam splitter (Thorlabs, CCM1-PBS251) was used to split the signal into the two ports of the balanced photodetector (Thorlabs, PDB210A). Each port was supplemented with NDF (Thorlabs, NE10A) that protected the photodiodes from power saturation and suppressed background noise. A continuously variable NDF (Thorlabs, NDC-50C-2M) in one of the arms was used to precisely balance the light intensity in both detector diodes.

We used a lock-in scheme to measure the Faraday rotation where the magnetic field was modulated by the local oscillator of a Zurich Instruments MFLI lock-in amplifier. We used a fourth order low pass filter with 0.8 s time constant to demodulate. A probe (Lakeshore, model 425 Gaussmeter) installed near the sample measured the magnetic field amplitude. To measure the magnetic field at the sample position, we used a terbium gallium garnet (TGG) crystal (MTI, TGGc1010S2) as a reference sample. Details of these calibration measurements can be found in supplementary material S2.

The intensities on the balanced detector photodiodes after Faraday rotation by an angle $\Delta\theta$ can be written as

$$I_1(t) = \alpha I' \cos(\theta + \Delta\theta(t))^2, \tag{2}$$

$$I_2(t) = \beta I' \sin(\theta + \Delta\theta(t))^2, \tag{3}$$

where I_1 and I_2 are the light intensities detected on the left and right photodiodes, θ is the angle between the incident light polarization and the PBS, which was set to 45°, I' is the total light intensity transmitted through the sample, and α and β are constants determined by the imperfect light intensity splitting between the two arms of the balanced photodetector. The constants α and β account for mirror losses, setup alignment, and photodiode balancing. The signal measured by the lock-in amplifier is the difference between the left and right photodiode signals

$$I_1(t) - I_2(t) = \frac{1}{2} I'(\alpha - \beta) - \frac{1}{2} I'(\alpha + \beta) \sin 2\Delta\theta(t) \tag{4}$$

and can be split into its alternating current (AC) and direct current (DC) components

$$I_{DC} = \frac{1}{2} I'(\alpha - \beta), \tag{5}$$

$$I_{AC}(t) = -\frac{1}{2} I'(\alpha + \beta) \sin 2\Delta\theta(t). \tag{6}$$

The Faraday rotation can be obtained from the ratio of the AC and DC components

$$\sin 2|\Delta\theta(t)| = \frac{\sqrt{2} I_{AC}(t)}{I_1 + I_2}, \tag{7}$$

where $\sqrt{2}$ arises from the root mean square (RMS) value of the AC signal, and I_1 and I_2 are measured without an applied magnetic field (see supplementary material S3 for more details).

The sample was prepared by depositing a 1 μm thick EuS film on a 0.5 mm thick silica substrate held at room temperature using electron beam evaporation. The base vacuum of the electron beam evaporator

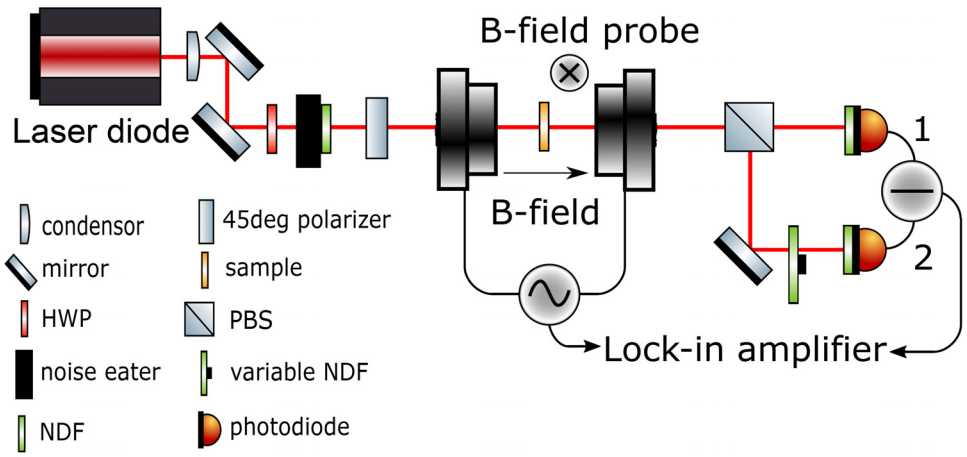

FIG. 1. Experimental setup for the Verdet constant measurements. The illumination source consists of a laser diode, noise eater, and polarizer. Input light intensity is controlled by adjusting a half-wave plate (HWP) and neutral density filter (NDF). An oscillating magnetic field (f = 1 Hz) periodically rotates the incident light's polarization. To measure the amplitude of these oscillations, we split light polarization into s- and p-components using a polarizing beam splitter (PBS). Then, a balanced photodetector measures the signal. The measured intensity difference is proportional to the Faraday rotation of the polarization axis, which is used to extract the Verdet constant.

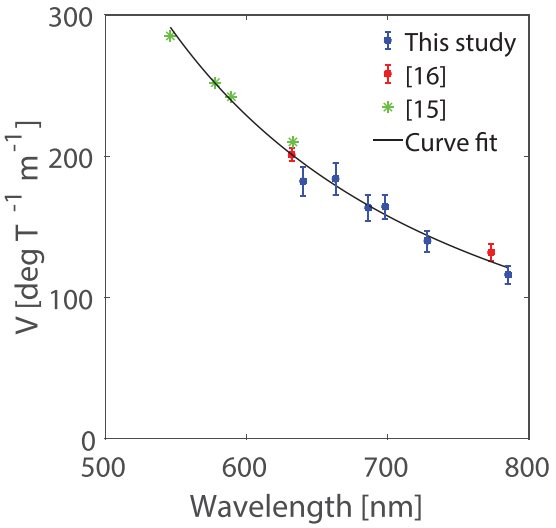

FIG. 2. Dispersion curve of the Verdet constant for the silica substrate. Verdet constants measured by other authors[15,16] are consistent with our measurements.

was ~6×10^{-8} Torr. A schematic of the sample is shown in the inset of Fig. 3(a). This sample was used to measure the Verdet constant of EuS. Although the Verdet constant of silica is small, the EuS film is three orders of magnitude thinner than the silica substrate. Therefore, we separately measured the Verdet constant of an identical silica substrate without the EuS film to account for the substrate contribution to the Faraday rotation. The results of the silica substrate measurements are shown in Fig. 2. The solid black line represents a fit of equation[14]

$$V = \frac{E}{\lambda^2 - \lambda_0^2} \tag{8}$$

to the measured data. E is a proportionality constant that depends on the concentration of the magnetic ions per volume, transition probability, and the Lande splitting factor, and λ_0 is a resonant transition wavelength for the paramagnetic ions. We extract the parameters $E = 65.8°\ \mu m^2\, T^{-1}\, m^{-1}$ and $\lambda_0 = 0.269\ \mu m$. We compared our results to the data obtained by other authors[15,16] (see Fig. 2). All datasets are in good agreement.

Using the measurement protocol described in supplementary material S3, we measured the dispersion of the Verdet constant of the EuS layer at room temperature. The results are plotted in Fig. 3(a). We fitted the measured data points using Eq. (8) and extracted $E = -10872$ deg $\mu m^2\, T^{-1}\, m^{-1}$ and $\lambda_0 = 0.5944\ \mu m$. We omitted the data point at $\lambda = 640$ nm for the fit due to its proximity to a material resonance.[19] For comparison, in Fig. 3(b), the Verdet constant dispersion curve of EuS measured at 6 K is plotted.[17] We observe similar qualitative behavior for both curves in Figs. 3(a) and 3(b). Both curves have a minimum between 650 and 700 nm. Figure 3(c) compares the measured EuS Verdet constant to the Verdet constant of TGG, which is commonly used in commercial isolators at visible wavelengths. EuS has an order of magnitude higher Verdet constant than TGG. Figure S4 compares the Faraday rotation and Faraday rotation normalized to attenuation of EuS with other common MO materials.

To measure the absorption of the EuS film, we performed spectroscopic ellipsometry (J. A. Woollam, -VASE32) measurements in the visible spectral range. The measurements were performed on a 100 nm thick film of EuS deposited on a half-inch square silicon wafer. The thickness of the EuS film was chosen to prevent Fabry–Pérot resonances in the measurement's spectral range. Si was selected as the sample substrate because the manufacturer of the spectroscopic ellipsometer recommends it for reliable data fitting. Raw ellipsometric data and tabulated refractive index values can be found in the supplementary material. The extracted refractive index and extinction coefficient are plotted in Fig. 4(a). The extinction coefficient of EuS does not exceed 0.15 in the wavelength range from 600 to 1000 nm but is higher than of TGG. However, it is much lower than that of metals. In comparison, the extinction coefficient of nickel[20] is above 3 in the discussed wavelength range.

The wavelength range of the Verdet constant studied in this work was chosen based on our absorption spectrum measurement of

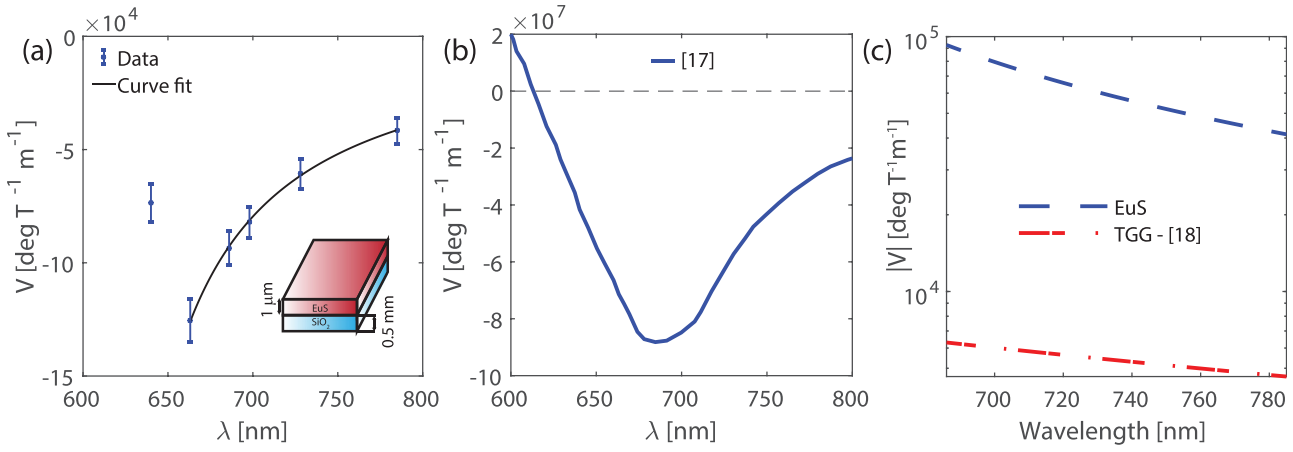

FIG. 3. Dispersion of the Verdet constant for EuS and its comparison to the TGG Verdet constant dispersion. (a) Measured Verdet constant dispersion of EuS at room temperature and a fit to the data. (b) Verdet constant of EuS at a temperature of 6 K.[17] The dashed line indicates zero. The room temperature dispersion of the Verdet constant of EuS has the same qualitative features as the Verdet constant measured at 6 K in the wavelength range between 600 and 800 nm. (c) The absolute value of the Verdet constants of the EuS film compared with TGG[18] at room temperature.

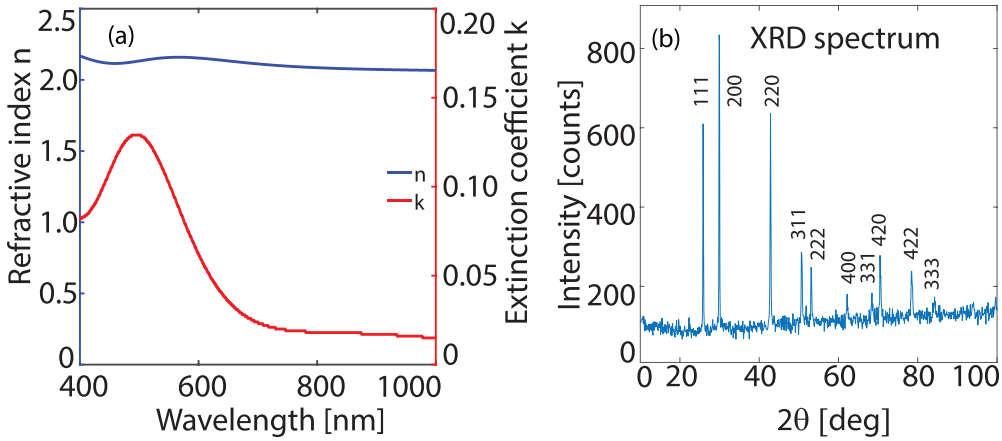

FIG. 4. Characterization of EuS. (a) The real and imaginary part of the refractive index of EuS extracted from ellipsometry measurements. (b) X-ray diffraction (XRD) measurement of EuS powder. Peaks show excellent agreement with the crystallographic database and confirm the purity of the used material.

EuS. Whereas the spectral maximum of the Verdet constant coincides with maximal absorption, low transmission prevents using the MO material close to this wavelength. Therefore, we concentrate on the tail of the absorption spectrum, where the Verdet constant is still very high, and absorption has already decayed.

To verify the purity of our EuS, we performed x-ray diffraction (XRD) analysis of the powder used for the fabrication of our sample [see Fig. 4(b)]. We found that the measured spectrum is in excellent agreement with the EuS XRD pattern available in the crystallographic database.[21]

This work presents measurements of the Verdet constant, refractive index, and extinction coefficient for a thin EuS film in the visible spectrum at room temperature. We found that the EuS film has an order of magnitude higher Verdet constant than the TGG crystal, which is commonly used in industry. In recent years, multiple ultrathin nanophotonic devices have been proposed to enhance the magneto-optical response per unit length.[22–26] These devices often rely on patterning magneto-optical materials or incorporating them into already patterned structures. Considering these devices, the fabrication simplicity of the MO material becomes an important parameter. Commonly used MO materials, such as TGG or yttrium gallium garnet (YIG), are tough to shape or deposit on top of certain substrates. Moreover, YIG loses part of its MO response when it is not crystalline. EuS can easily be evaporated on top of patterned structures without losing its MO properties, making it an exciting material despite its moderate absorption values. Nickel deposited on top of silicon Mie resonators greatly enhances their MO response with a slight transmission loss.[22] Introducing EuS in such a system is expected to decrease the intensity loss even further.

See the supplementary material for additional data and analysis.

This work was supported by the Air Force Office of Scientific Research under Award No. FA9550-19-1-0352. M. Ossiander is supported by a Feodor-Lynen Fellowship from the Alexander von Humboldt Foundation. The work at MIT was supported by Army Research Office (No. ARO W911NF-20-2-0061), the National Science Foundation (No. NSF-DMR 1700137), Office of Naval Research (No. N00014-20-1-2306), and the Center for Integrated Quantum Materials (No. NSF-DMR 1231319). This work was performed in part at the Harvard University Center for Nanoscale Systems (CNS); a member of the National Nanotechnology Coordinated Infrastructure Network (NNCI), which is supported by the National Science Foundation under NSF Award No. ECCS-2025158.

AUTHOR DECLARATIONS

Conflict of Interest

The authors have no conflicts to disclose.

Author Contributions

M. L. Meretska: Conceptualization (lead); Data curation (lead); Formal analysis (equal); Methodology (lead); Software (equal); Supervision (lead). **F. H. B. Somhorst:** Investigation (equal); Writing – original draft (equal); Writing – review and editing (equal). **M. Ossiander:** Methodology (supporting); Writing – original draft (equal); Writing – review and editing (equal). **Y. Hou:** Resources (lead); Writing – original draft (equal); Writing – review and editing (equal). **J. Moodera:** Resources (lead); Writing – original draft (equal); Writing – review and editing (equal). **F. Capasso:** Data curation (equal); Funding acquisition (lead); Supervision (lead); Writing – original draft (equal); Writing – review and editing (equal).

DATA AVAILABILITY

The data that support the findings of this study are available from the corresponding authors upon reasonable request.

REFERENCES

[1]E. Hecht, *Optics* (Pearson, 2012).
[2]V. A. Zvezdin and A. K. Kotov, *Modern Magnetooptics and Magnetooptical Materials* (CRC Press, 2020).
[3]V. A. Kastler, "50 Jahre Hanle-Effekt: Rückblick und Vorblick," Phys. Bl. **30**(9), 394–404 (1974).

[4]B. Sepúlveda, G. Armelles, and L. M. Lechuga, "Magneto-optical phase modulation in integrated Mach–Zehnder interferometric sensors," Sens. Actuators, A **134**(2), 339–347 (2007).
[5]D. Huang, P. Pintus, C. Zhang *et al.*, "Dynamically reconfigurable integrated optical circulators," Optica **4**(1), 23–30 (2017).
[6]Q. Du, C. Wang, Y. Zhang *et al.*, "Monolithic on-chip magneto-optical isolator with 3 dB insertion loss and 40 dB isolation ratio," ACS Photonics **5**(12), 5010–5016 (2018).
[7]D. S. Bulgarevich, Y. Akamine, M. Talara *et al.*, "Terahertz magneto-optic sensor/imager," Sci. Rep. **10**(1), 1–7 (2020).
[8]S. Hua, J. Wen, X. Jiang *et al.*, "Demonstration of a chip-based optical isolator with parametric amplification," Nat. Commun. **7**(1), 1–6 (2016).
[9]D. Jalas, A. Petrov, M. Eich *et al.*, "What is—and what is not—an optical isolator," Nat. Photonics **7**(8), 579–582 (2013).
[10]N. Parappurath, F. Alpeggiani, L. Kuipers *et al.*, "The origin and limit of asymmetric transmission in chiral resonators," ACS Photonics **4**(4), 884–890 (2017).
[11]D. Floess and H. Giessen, "Nonreciprocal hybrid magnetoplasmonics," Rep. Prog. Phys. **81**(11), 116401 (2018).
[12]*The Physics of Opto-Electronic Materials: Proceedings of the Symposium on the Physics of Opto-Electronic Materials*, edited by W. A. Albers (Springer, 1971), p. 281.
[13]J. O. Dimmock, "Magneto-optical properties of the Eu-chalcogendes," in *The Physics of Opto-Electronic Materials* (Springer, 1971), pp. 255–271.
[14]J. Y. Jo, Y. Kim, C. K. Hwangbo *et al.*, "Sensitive measurement of the magneto-optic effect in the near infrared wavelength region with weak alternating magnetic fields," Opt. Mater. Express **8**(9), 2636 (2018).
[15]G. Phelps, J. Abney, M. Broering *et al.*, "A sensitive Faraday rotation setup using triple modulation," Rev. Sci. Instrum. **86**, 073107 (2015).
[16]W. B. Garn, R. S. Caird, C. M. Fowler *et al.*, "Measurement of Faraday rotation in megagauss fields over the continuous visible spectrum," Rev. Sci. Instrum. **39**(9), 1313–1317 (1968).
[17]G. Güntherodt, J. Schoenes, and P. Wachter, "Optical constants of the Eu chalcogenides above and below the magnetic ordering temperatures," J. Appl. Phys. **41**(3), 1083–1084 (1970).
[18]E. G. Víllora, P. Molina, M. Nakamura *et al.*, "Faraday rotator properties of $\{Tb_3\}[Sc_{1.95}Lu_{0.05}](Al_3)O_{12}$, a highly transparent terbium-garnet for visible-infrared optical isolators," Appl. Phys. Lett. **99**(1), 011111 (2011).
[19]D. Vojna, O. Slezák, A. Lucianetti *et al.*, "Verdet constant of magneto-active materials developed for high-power Faraday devices," Appl. Sci. **9**(15), 3160 (2019).
[20]P. B. Johnson and R. W. Christy, "Optical constants of transition metals: Ti, V, Cr, Mn, Fe, Co, Ni, and Pd," Phys. Rev. B **9**(12), 5056 (1974).
[21]K. Persson, see https://materialsproject.org/materials/mp-20587/ for "Materials Data on EuS (SG:225) by Materials Project" (last accessed January 20, 2022).
[22]M. G. Barsukova, A. S. Shorokhov, A. I. Musorin *et al.*, "Magneto-optical response enhanced by Mie resonances in nanoantennas," ACS Photonics **4**(10), 2390–2395 (2017).
[23]G. Armelles, J. Bautista González-Díaz, A. García-Martín *et al.*, "Localized surface plasmon resonance effects on the magneto-optical activity of continuous Au/Co/Au trilayers," Opt. Express **16**(20), 16104–16112 (2008).
[24]T. Kiel, P. Varytis, B. Beverungen *et al.*, "Enhanced Faraday rotation by dielectric metasurfaces with Bayesian shape-optimized scatterers," Opt. Lett. **46**(7), 1720–1723 (2021).
[25]M. Inoue, K. Arai, T. Fujii *et al.*, "One-dimensional magnetophotonic crystals," J. Appl. Phys. **85**, 5768 (1999).
[26]M. Decker, I. Staude, M. Falkner *et al.*, "High-efficiency dielectric Huygens' surfaces," Adv. Opt. Mater. **3**(6), 813–820 (2015).